Angle-dependent thermodynamics of α-$RuCl_3$

S. Bachus,[1,*] D. A. S. Kaib,[2,†] A. Jesche,[1] V. Tsurkan,[3,4] A. Loidl,[3] S. M. Winter,[5,‡] A. A. Tsirlin,[1,§] R. Valentí,[2,‖] and P. Gegenwart[1,¶]

[1]*Experimental Physics VI, Center for Electronic Correlations and Magnetism, University of Augsburg, 86159 Augsburg, Germany*
[2]*Institute of Theoretical Physics, Goethe University Frankfurt, 60438 Frankfurt am Main, Germany*
[3]*Experimental Physics V, Center for Electronic Correlations and Magnetism, University of Augsburg, 86159 Augsburg, Germany*
[4]*Institute of Applied Physics, Chisinau MD-2028, Republic of Moldova*
[5]*Department of Physics and Center for Functional Materials, Wake Forest University, Winston-Salem, North Carolina 27109, USA*

(Received 18 December 2020; revised 4 February 2021; accepted 5 February 2021; published 26 February 2021)

Thermodynamics of the Kitaev honeycomb magnet α-$RuCl_3$ is studied for different directions of in-plane magnetic field using measurements of the magnetic Grüneisen parameter Γ_B and specific heat C. We identify two critical fields B_c^{AF1} and B_c^{AF2} corresponding, respectively, to a transition between two magnetically ordered states and the loss of magnetic order toward a quantum paramagnetic state. The B_c^{AF2} phase boundary reveals a narrow region of magnetic fields where inverse melting of the ordered phase may occur. No additional transitions are detected above B_c^{AF2} for any direction of the in-plane field, although a shoulder anomaly in Γ_B is observed systematically at 8–10 T . Large field-induced entropy effects imply additional low-energy excitations at low fields and/or strongly field-dependent phonon entropies. Our results establish universal features of α-$RuCl_3$ in high magnetic fields and challenge the presence of a field-induced Kitaev spin liquid in this material.

DOI: 10.1103/PhysRevB.103.054440

I. INTRODUCTION

The Kitaev honeycomb model offers a possible practical route toward a quantum spin liquid with exotic fractionalized excitations and potential applications in topological quantum computing [1,2]. The 4*d* layered honeycomb material α-$RuCl_3$ is one of the best experimental realizations of this model available so far [3–5]. However, it develops long-range magnetic order in zero magnetic field and may only be proximate to the elusive Kitaev spin liquid (KSL) [6,7]. Tuning α-$RuCl_3$ by pressure [8,9] or chemical substitution [10] is hampered by unwanted effects of dimerization and magnetic dilution, respectively. On the other hand, magnetic fields applied within the honeycomb (*ab*) plane can act as a very clean tuning mechanism that eliminates magnetic order above $B_c = 7.0$–7.5 T [11–13].

The physics within this region without magnetic order are the subject of significant debate. On one hand, a half-integer plateau in the thermal Hall conductivity (THC) as expected for the KSL phase has been reported [14]. However, spectroscopic measurements find excitations that are expected for the topologically trivial, partially-polarized phase [15–17]. To scrutinize this, recent studies compared the effects from rotating the magnetic field within the plane against the expectations for the KSL.

For the Kitaev model under *most* in-plane field angles ϕ, the KSL would be gapped and show a quantized THC with ϕ-dependent sign. Yet for fields parallel to a bond ($\phi = n \times 60^\circ$, $n \in \mathbb{Z}$ [18]), the KSL would be gapless and show no THC. Experimentally, the sign structure of the THC was indeed observed in α-$RuCl_3$ [19]. However, for in-plane fields, the same sign structure is expected for the partially-polarized phase, suggesting that the dependence of the THC with ϕ alone at the accessed temperatures cannot distinguish between the scenarios [20]. The gaplessness of the field-induced state for distinct ϕ (as predicted for the KSL), however, would be a property clearly incompatible with the partially-polarized phase. Accordingly, the ϕ-dependent gap was recently investigated by Tanaka *et al.* [21]. From analysis of their low-temperature specific heat measurements, a gapless behavior for $\phi = n \times 60^\circ$ and gapped behavior for $\phi \neq n \times 60^\circ$, as expected for the KSL, was reported [21].

Another pertinent question is the occurrence of a phase transition upon entering and leaving this putative QSL as a function of field. No conspicuous signatures of such transitions are found in recent studies using various thermodynamic probes [22,23]. Here, we employ the magnetic Grüneisen parameter (Γ_B) and specific heat (C) to map out the field-angle, field-strength, and temperature-dependent phase diagram of α-$RuCl_3$. These demonstrate the absence of further phase transitions beyond the magnetically ordered region for *any* in-plane angle of the magnetic field. We furthermore uncover a finite region where inverse melting of the antiferromagnetic phase may occur and track shoulder anomalies in Γ_B within the quantum paramagnetic region. In addition, the

*sebastian.bachus@physik.uni-augsburg.de
†kaib@itp.uni-frankfurt.de
‡winters@wfu.edu
§altsirlin@gmail.com
‖valenti@itp.uni-frankfurt.de
¶philipp.gegenwart@physik.uni-augsburg.de

combination of Γ_B and C allows us to directly resolve entropy differences between states at different field strengths and angles. These reveal an unexpectedly large loss of entropy from the zero-field gapped ordered phases to the quantum paramagnetic region, independent of in-plane angle of the field.

II. METHODS

A. Experimental details

The field-dependent measurements of specific heat (C) and magnetic Grüneisen parameter (Γ_B) were performed in a dilution refrigerator using the relaxation method for C (see Appendix B) and the high-resolution alternating-field method for Γ_B [24]. The background of the cell was subtracted from the raw data, unless stated otherwise. The magnetic field orientation in the honeycomb plane of α-$RuCl_3$ was adjusted by tilting the cell, including the sample platform, using brass wedges with different angles [Fig. 1(a)]. The crystal with a thickness of $\sim$1 mm was mounted with the honeycomb planes parallel to the platform, and the cell was attached to the cryostat sample holder, such that the magnetic field direction was always within the plane. Rotating the cell by the wedges results in a variation of the in-plane field angle. This way, we measured several configurations and determined the critical fields $B_c^{\mathrm{AF1,2}}$. By comparing these results to ac-susceptibility measurements [25], we calibrated our field orientation relative to the [010] direction which we defined as $\phi = 0^\circ$. Here, we used the near sixfold symmetry which has further been validated by the angle dependency of specific heat [21]. Note that our previously measured field direction $\phi = 20^\circ$ [23] used a slightly modified setup. Strictly speaking, this corresponded to a value of $\phi = 100^\circ$, which is equivalent to $\phi = 20^\circ$ in the angle-field phase diagram (Fig. 2). In the same way, $\phi = -5^\circ$ is equivalent to $\phi = +5^\circ$. The excellent agreement of our angle-field phase diagram with the ac-susceptibility measurements further approves the sixfold symmetry of the B_c^{AF1} and B_c^{AF2} transitions.

Samples with a small heat capacity compared to that of the cell require a careful background subtraction for the Grüneisen parameter Γ_B. First, the total value $\Gamma_{B,\mathrm{tot}}$ has to be measured which includes both cell and sample contributions. Second, the heat capacities C_{Sa} and C_{Cell} of, respectively, the sample and cell are needed. Together with $\Gamma_{B,\mathrm{Cell}}$, the sample's Grüneisen parameter is calculated according to Ref. [23]:

$$\Gamma_{B,\mathrm{Sa}} = \Gamma_{B,\mathrm{tot}} + \frac{C_{\mathrm{Cell}}}{C_{\mathrm{Sa}}}(\Gamma_{B,\mathrm{tot}} - \Gamma_{B,\mathrm{Cell}}). \quad (1)$$

As a result, the background subtraction is not feasible in the absence of $C(B)$. Considering huge time requirements for such a measurement, as opposed to the measurement of Γ_B, we chose not to perform it for each temperature and field direction and used the raw data in our analysis.

In Fig. 1(b), we exemplarily show background subtraction for Γ_B at 1 K. One sees that the cell background is negligible in the vicinity of B_c^{AF1} and B_c^{AF2}, so the raw data can be safely used for the determination of critical fields. The background contribution becomes more significant above B_c^{AF2}, where specific heat of the sample decreases. Here, the background is responsible for the apparent negative values of Γ_B above

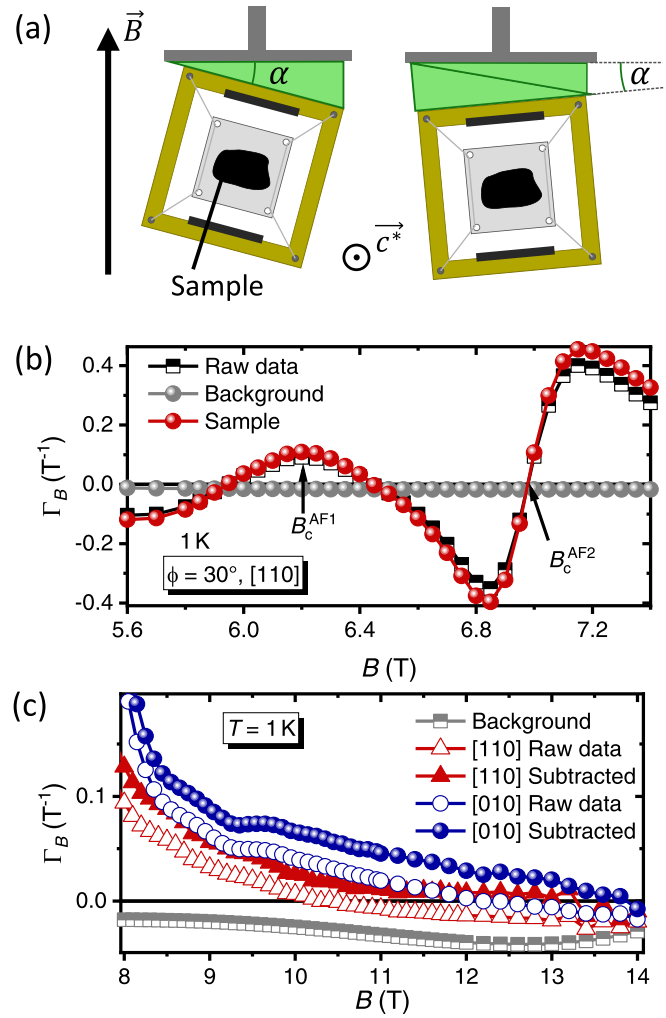

FIG. 1. (a) Rotation of Grüneisen and specific heat setup by using brass wedges ($\vec{c}^*$ perpendicular to sample platform, magnetic field orientation indicated in the sketch). Note that α is not equivalent to ϕ which is assigned by comparing the critical fields to ac-susceptibility measurements (Fig. 2). (b) Cell background subtraction for $\vec{B} \parallel [110]$ at 1 K following Eq. (1). Raw data denote the Grüneisen parameter from both cell and sample. For the background measurement, $\Gamma_{B,\mathrm{Cell}}$ was measured independently with magnetic field applied perpendicular to the cell platform. Since no field dependency is expected for the cell, all subtractions use the same background measurement. Despite the subtraction, the positions of B_c^{AF1} and B_c^{AF2} are unaffected. (c) At high fields far beyond B_c^{AF2}, the background is responsible for the negative Γ_B values. The characteristics of $\Gamma_B(B)$, however, are again untouched by the background subtraction.

10–12 T, while positive values are recovered once the background contribution is subtracted [Fig. 1(c)]. Therefore, we argue that Γ_B of the sample remains positive even well above B_c^{AF2}. We also note that, should any phase transitions occur above B_c^{AF2}, they would of course show up also in the raw data.

The same high-quality single crystal as in Ref. [23] was used. It was grown by vacuum sublimation [26], and its quality was checked by heat capacity as well as susceptibility measurements [23].

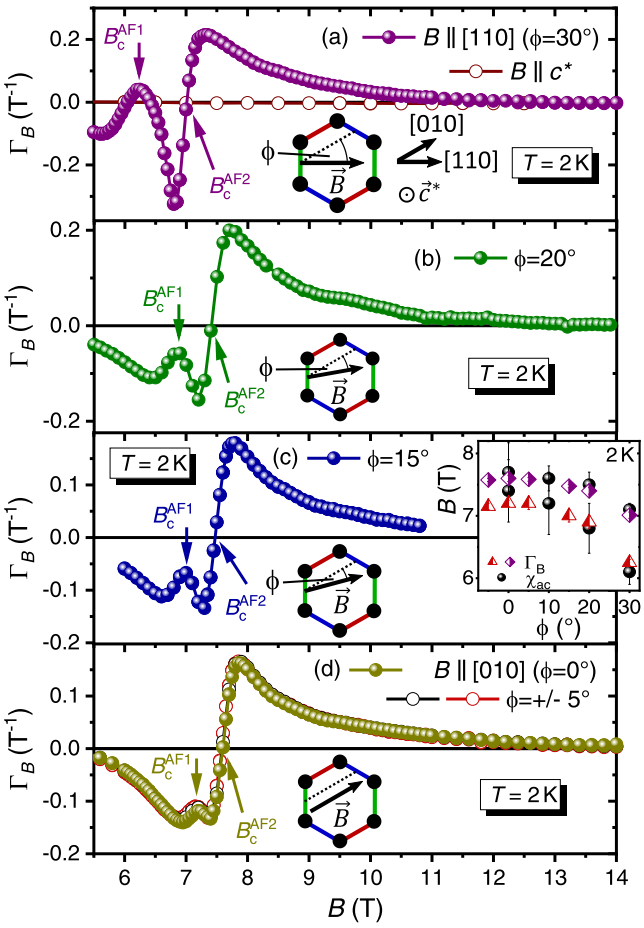

FIG. 2. Angle dependence of the magnetic Grüneisen parameter Γ_B at 2 K (raw data). The critical fields of the phase transitions B_c^{AF1} and B_c^{AF2} are shifted for different in-plane field orientations, from (a) $\vec{B} \parallel [110]$ to (d) $\vec{B} \parallel [010]$; the data for $\phi = 20^\circ$ are from Ref. [23]. The inset in (c) shows the excellent agreement with the critical fields determined from ac-susceptibility measurements [25]. No further phase transitions are observed above B_c^{AF2} for all field directions up to at least 14 T. The measurement perpendicular to the honeycomb plane ($\vec{B} \parallel \vec{c}^*$) in (a) excludes any out-of-plane contribution.

B. Model for exact diagonalization

To compare our measurements of Γ_B to expectations from extended Kitaev models, we employ exact diagonalization on a two-dimensional 24-sites honeycomb cluster with C_3 symmetry. To access Γ_B at small finite temperatures, we follow the method applied for the theoretical calculations in Ref. [23]. While these two-dimensional calculations cannot capture the transition B_c^{AF1} related to the change of the out-of-plane ordering wave vector, other properties like B_c^{AF2}, the magnitude and sign of Γ_B, and possible occurrences of shoulder anomalies may be compared qualitatively.

In extended Kitaev models, the three nearest-neighbor bonds of the honeycomb lattice are defined as X_1, Y_1, Z_1 bonds depending on their orientation. Second-neighbor X_2, Y_2, Z_2 (third-neighbor X_3, Y_3, Z_3) bonds within the plane are then defined as those orthogonal (parallel) to the directions of the respective X_1, Y_1, Z_1 bonds. The effective magnetic Hamiltonian for Z_n bonds ($n \in \{1, 2, 3\}$) then reads

$$H_{\mathrm{Z}_n} = \sum_{\langle ij \rangle_{\mathrm{Z}_n}} \left[J_n \mathbf{S}_i \cdot \mathbf{S}_j + K_n S_i^z S_j^z + \Gamma_n \left(S_i^x S_j^y + S_i^y S_j^x \right) + \Gamma_n' \left(S_i^x S_j^z + S_i^z S_j^x + S_i^y S_j^z + S_i^z S_j^y \right) \right], \quad (2)$$

with effective spin-$\frac{1}{2}$ operators $\mathbf{S}_i$. The Hamiltonians for X_n and Y_n bonds can be obtained by cyclic permutation of spin components (x, y, z) in Eq. (2). Furthermore, a Zeeman term $H_{\mathrm{Zee}} = -\mu_B \sum_i \mathbf{B} \cdot \mathbf{g} \cdot \mathbf{S}_i$ can contribute with magnetic field $\mathbf{B}$ and the g-tensor $\mathbf{g}$. If K_1 is the only finite exchange coupling and $B = 0$, the model reduces to the exactly solvable Kitaev honeycomb model.

III. RESULTS

A. Inverse melting at critical fields $B_c^{\mathrm{AF1/2}}$

In Fig. 2, we show the measured field dependence of $\Gamma_B(B) = -(\partial M/\partial T)/C$ up to 14 T for several in-plane field directions. We also performed a measurement with the field perpendicular to the *ab* plane ($\vec{B} \parallel \vec{c}^*$) that returned $\Gamma_B \approx 0$ up to 14 T [empty circles in Fig. 2(a)]. This behavior is to be expected since no field-induced transitions should occur in the out-of-plane field within the field range of our study [12,27–29], and even the Néel temperature of α-$\mathrm{RuCl_3}$ does not change appreciably. This confirms that all features observed in our measurements arise from in-plane fields and cannot be caused by sample misalignment.

Our data shows two phase transitions as a function of field strength. The dominant feature is the sign change of Γ_B from negative to positive at B_c^{AF2}, which is equivalent to an entropy maximum at a second-order phase transition. It marks the phase boundary between the long-range-ordered and quantum paramagnetic regions of α-$\mathrm{RuCl_3}$. A somewhat weaker signature identifies B_c^{AF1} as a first-order transition between two different antiferromagnetically (AF) ordered states [10] caused by a change in out-of-plane ordering [25]. In this case, the transition point is determined by a maximum in $\Gamma_B(B)$, which is equivalent to a smeared negative step in the entropy. Note that Fig. 2 depicts the raw data of $\Gamma_B(B)$ since subtraction of the cell background was not possible for all curves. This neither affects the values of the critical fields $B_c^{\mathrm{AF1,2}}$, nor changes the evolution of Γ_{mag} at high fields that will be discussed in Sec. III B.

Rotating the field strongly influences the positions of both B_c^{AF1} and B_c^{AF2}, illustrating the in-plane anisotropy of the system [compare Figs. 2(a)–2(d)]. This anisotropy is most pronounced for the [110]-direction [Fig. 2(a)], where already small changes of ϕ influence $B_c^{\mathrm{AF1,2}}$. Both absolute values of the critical fields and their angular dependence match perfectly the results of previous ac-susceptibility (χ') measurements [25], where critical fields were determined from peaks in χ'. This validates our procedure for the evaluation of B_c^{AF1} and B_c^{AF2} and allows their measurement over a broad temperature range, as Γ_B is generally more sensitive to field-induced phase transitions than, e.g., specific heat.

We will take advantage of this unique sensitivity to probe the presence of field-induced phase transitions above B_c^{AF2}, but first we discuss peculiarities of the critical fields B_c^{AF1},

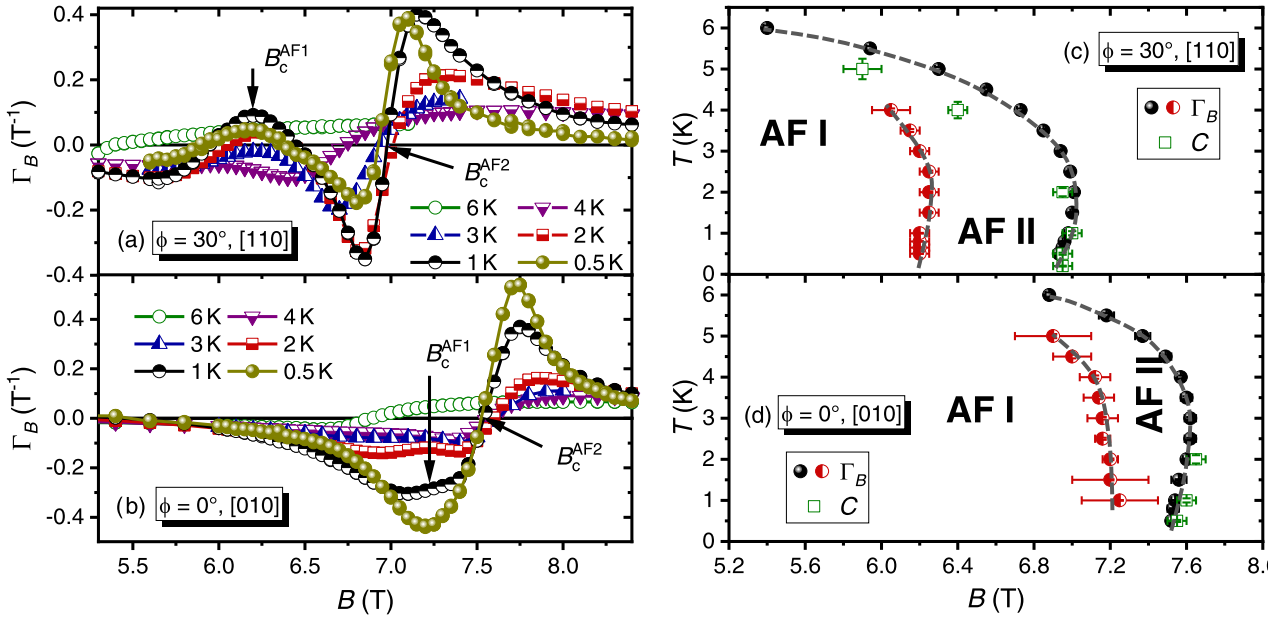

FIG. 3. Field dependence of the magnetic Grüneisen parameter Γ_B (raw data) for several temperatures with the in-plane magnetic field $\vec{B}$ applied parallel (a) to [110] and (b) to [010]. B_c^{AF2} is the point where Γ_B changes sign upon the transition between long-range-ordered and quantum paramagnetic states of α-$RuCl_3$ [23]. At higher temperatures, B_c^{AF2} shifts towards lower fields due to thermal fluctuations. However, below 2 K an opposite behavior is observed, suggesting that the phase boundary is nonmonotonic [(c),(d)]. The phase transition inside the AF state at B_c^{AF1} is most likely of first order and, thus, manifests itself in a maximum of Γ_B, which is clearly visible for $\vec{B} \parallel [110]$. By increasing the temperature the maximum is suppressed and gradually shifted toward lower fields. A very similar behavior is observed for $\vec{B} \parallel [010]$, yet the determination of B_c^{AF1} is significantly more difficult due to the proximity to B_c^{AF2} (see Appendix A).

B_c^{AF2} as a function of temperature. Figure 3(a) shows the field-dependent raw data of Γ_B for several temperatures and the field applied along the [110] direction. For $T \geqslant 2$ K, the critical field B_c^{AF2} (marked by the sign change of Γ_B) shifts to lower fields with increasing temperature. This behavior is expected, since the stability of a symmetry-broken phase ($B < B_c^{AF2}$) is usually decreased by thermal fluctuations. However, below 2 K an opposite behavior is observed, resulting in the nonmonotonic phase boundary of B_c^{AF2} [Fig. 3(c)]. A very similar temperature dependence of B_c^{AF2} is also detected for $\vec{B} \parallel [010]$ [Figs. 3(b) and 3(d)] and verified by independent specific heat measurements, where B_c^{AF2} manifests itself by a peak (Fig. 4). Below 2 K, we find excellent agreement between the B_c^{AF2} values from Γ_B and C. At higher temperatures, the peak in the specific heat broadens, and the determination of B_c^{AF2} from the peak position becomes less accurate than from the sign change in Γ_B. Temperature dependence of B_c^{AF1} shows an overall similar behavior, except for the fact that the temperature dependence of B_c^{AF1} is monotonic for $\vec{B} \parallel [010]$.

The peculiarities of the phase boundaries are independently confirmed by field dependence of the magnetic entropy obtained as $\Delta S = -\int dB\, \Gamma_B C$ using the Maxwell equation $(\partial S/\partial B) = (\partial M/\partial T)$ (Fig. 4). The Clausius-Clapeyron equation requires that $dB_c^{AF1}/dT = -\Delta S/\Delta M$, where ΔS and ΔM are changes in, respectively, entropy and magnetization across the transition. Since $\Delta M > 0, dB_c^{AF1}/dT > 0$ implies a negative contribution in the entropy due to B_c^{AF1} [$\Delta S_c^{AF1} < 0$], and indeed we observe the reduction in ΔS around B_c^{AF1} for $\vec{B} \parallel [110]$ [Fig. 4(a)] but not for $\vec{B} \parallel [010]$ [Fig. 4(b)].

As likely no symmetry is broken for $B > B_c^{AF2}$, the nonmonotonic phase boundary implies a narrow range of magnetic fields, near 7.0 T for $\vec{B} \parallel [110]$ and 7.6 T for

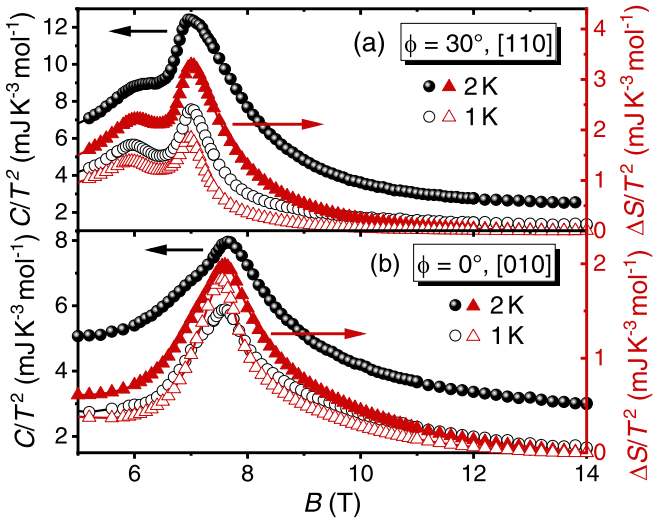

FIG. 4. Field dependence of specific heat C and entropy increment ΔS for in-plane fields parallel to (a) [110] and (b) [010] at 1 and 2 K, scaled by T^2 for better comparison. No signature for any phase transition beyond B_c^{AF2} is visible up to 14 T. The most prominent part arises from the peak at the phase transition B_c^{AF2} for both field directions. While B_c^{AF1} can also be identified in (a) $C(B)$ and $\Delta S(B)$ by another peak, respectively, it is not pronounced in the measurements for (b), most likely due to the closeness to B_c^{AF2}.

$\vec{B} \parallel [010]$, where the system upon cooling first enters a magnetically ordered state (AF2) and at lower temperatures becomes disordered again. Such *inverse melting* behavior has been predicted theoretically for some anisotropic spin models [30–32]. It may therefore be an interesting future avenue for theory to also search for inverse melting in extended Kitaev models.

From the integrated entropy differences, we note that the total observed field-induced entropy release from zero field, $S(0\,\mathrm{T}) - S(14\,\mathrm{T}) \approx 0.65\,\mathrm{mJ\,mol^{-1}\,K^{-1}}$ (here at $T = 1$ K, $\phi = 0°$), appears to be much larger than the maximum *magnetic* entropy that one would expect in the zero-field antiferromagnetic phase with a gap $\Delta > 1.5$ meV (inferred from inelastic neutron scattering [13,33]) [34]. Therefore, there are either additional low-energy magnetic excitations at $B = 0$ below the resolution of neutron scattering [35,36], and/or the significant magnetoelastic coupling of α-$RuCl_3$ [22,36–38] leads to a strongly field-dependent phonon entropy through magnetostriction-type effects.

B. Beyond magnetic order ($B > B_c^{AF2}$)

Having established boundaries of the magnetically ordered phases in α-$RuCl_3$, we now proceed to the evolution of the system in the quantum paramagnetic region above B_c^{AF2}. Here, several measurements of thermal Hall effect reported the half-integer plateau [14,19,39]—at ∼9 T to ∼11.5 T for $\vec{B} \parallel [110]$ [19]—and also suggested an extreme sensitivity of this measurement to the sample quality [39]. If this thermal Hall plateau originates from a gapped topological KSL as suggested by these reports, phase transitions to the bordering topologically trivial phases should occur. These would happen either through gap closing or be first order. Our data firmly excludes the former possibility for α-$RuCl_3$, since no sign change from negative to positive is observed in Γ_B above B_c^{AF2} at any field direction (Fig. 2) and temperatures down to 0.5 K (Fig. 5). Instead, Γ_B appears to asymptotically approach zero at high field strengths for all angles (Fig. 2), which would be consistent with the behavior of a single partially-polarized phase above B_c^{AF2}. Before discussing the alternative scenario of a first-order transition out of a putative KSL, we inspect Γ_B for further possible anomalies aside from sign changes.

The only conspicuous feature in Γ_B at 1 K above B_c^{AF2} is a shoulder for $\vec{B} \parallel [010]$, setting in at 9.3 T (Fig. 5, yellow symbols). This can be paralleled to similar weak anomalies reported previously in the magnetocaloric effect ($\phi = 20°$) [40] and magnetostriction ([010]) [37]. In contrast, for $\vec{B} \parallel [110]$, no clear shoulder is visible. However, a rather abrupt change of slope at ∼8.2 T is present (Fig. 5, magenta dotted line), which can be interpreted as a shoulder superimposed on the rapidly decreasing $\Gamma_B \sim 1/(B - B_c^{AF2})$ in the vicinity of B_c^{AF2} due to critical fluctuations [41]. Interestingly, a similar feature can be identified for [010], too (Fig. 5, yellow dotted lines). By reducing the temperature to 0.5 K, these anomalies become more prominent, possibly with two shoulders for $\vec{B} \parallel [010]$ (inset Fig. 5). Previously, we assigned such a shoulder feature to a level crossing in low-energy excitations [23]. Our data in Fig. 5 suggest that the field strength at which this occurs has only a weak dependence on the in-plane field direction, qualitatively consistent with an *ab-initio*-derived microscopic

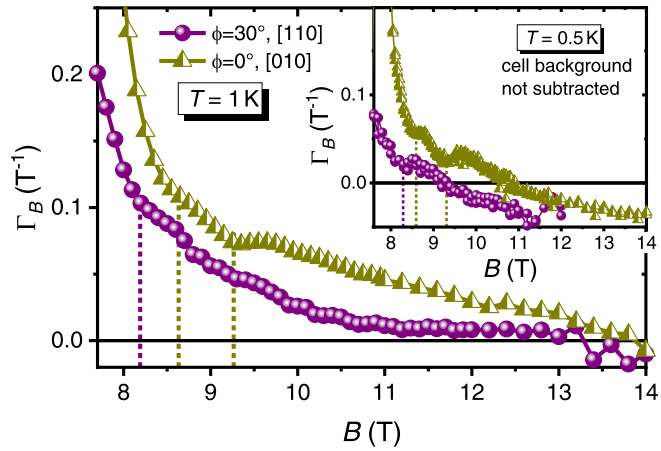

FIG. 5. Closeup of high-field part of Γ_B at 1 K. Any purported phase transition is absent above B_c^{AF2} up to 14 T, and Γ_B goes to zero due to very tiny remaining entropy (Fig. 4). The shoulder reported in Ref. [23] for $\phi = 20°$ indicative for excited level crossing is also visible for $\vec{B} \parallel [010]$, roughly setting in at the same position of ∼9.3 T. Additionally, a weaker second kink is present at 8.6 T. For $\vec{B} \parallel [110]$ a similar change of slope can be identified at ∼8.2 T as the only anomaly above B_c^{AF2}. Shown in the inset, the measurements at 0.5 K confirm the aforementioned results with the lacking phase transition and the more clearly visible anomalies. Note that the negative values of Γ_B are caused by the cell background, which could not be subtracted at 0.5 K.

model of α-$RuCl_3$ [38], see Sec. III C. This observation is also in line with recent spectroscopic measurements suggesting only a weak dependence of Γ-point ($\mathbf{q} = 0$) excitations on the direction of the in-plane field [16,42].

While we ruled out a continuous transition above B_c^{AF2}, we now investigate the possibility of whether these anomalies and/or other features in our data could support a first-order transition out of a KSL phase. Such a first-order scenario was put forward recently [21], where both the putative gapless ($\phi = 0°$) and gapped ($\phi \neq 0°$) KSLs would experience first-order transitions towards a gapped topologically trivial phase at $B \gtrsim 10$ T. We therefore examine field-dependent entropy changes, obtained as $\Delta S = -\int dB\, \Gamma_B C$. These are shown for $\phi = 30°$ and $\phi = 0°$ in Fig. 4, where each entropy curve has been shifted such that $\Delta S(14\,\mathrm{T}) = 0\,\mathrm{mJ\,K^{-1}\,mol^{-1}}$.

No anomalies are detected in ΔS above B_c^{AF2} for either field direction and up to 14 T. For $\phi = 30°$, the gap within the putative KSL would be the largest, such that a first-order transition to another phase with comparable gap may be hard to detect. However, for the putative gapless KSL along $\phi = 0°$, one would expect significant latent heat to be released at a first-order transition to a gapped state, which we however do not observe. Instead, entropy appears to shrink asymptotically with field strength, consistent with a continuously growing gap in a single partially-polarized phase above B_c^{AF2}.

C. Comparison to exact diagonalization results

We discuss two representative models that have been shown to be qualitatively consistent with numerous experimental observations in α-$RuCl_3$. Figures 6(a) and 6(b) show results for Γ_B for the minimal model of Refs. [43,44] (from here on "model A"), whose nonzero magnetic

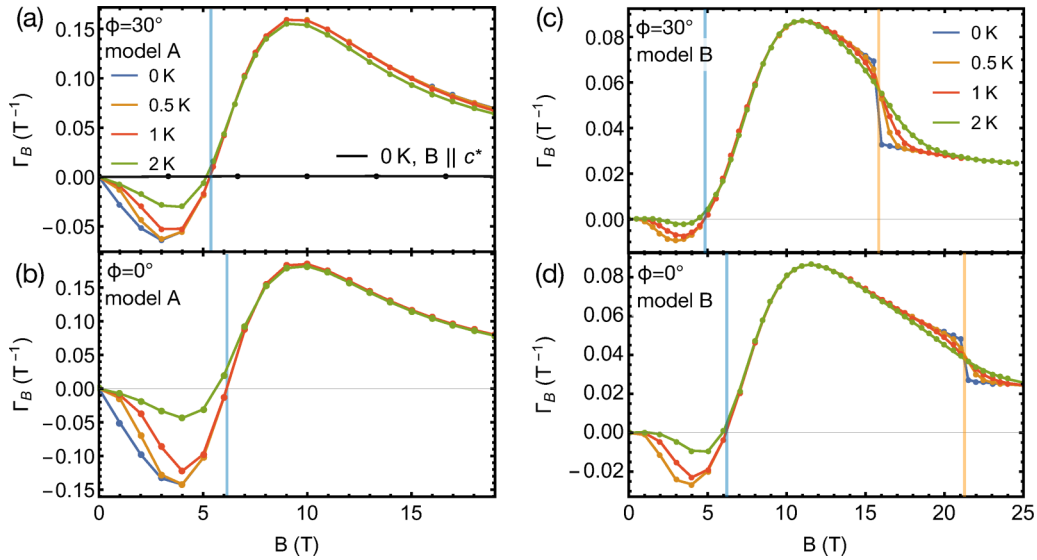

FIG. 6. Numerical results for Γ_B in two extended Kitaev models and different field directions. Blue vertical lines mark sign changes in Γ_B; orange lines mark shoulder anomalies. (a),(b) Results for the model of Refs. [43,44] ("model A"). (c),(d) Results for the model of Ref. [38] ("model B"), whose small second-neighbor J_2 and Dzyaloshinskii-Moriya interactions were neglected.

couplings are $(J_1, K_1, \Gamma_1, J_3) = (-0.5, -5, 2.5, 0.5)$ meV and where $(g_{ab}, g_{c^*}) = (2.3, 1.3)$. Figures 6(c) and 6(d) show results of the *ab initio* derived model of Ref. [38] ("model B"), $(J_1, K_1, \Gamma_1, \Gamma_1', K_2, \Gamma_2, \Gamma_2', J_3, K_3, \Gamma_3, \Gamma_3') = (-5.66, -10.12, 9.35, -0.73, -0.18, 0.06, 0.03, 0.2, 0.25, 0.04, -0.07)$ meV and $g_{ab} = 2.36$, where we omitted weak second-neighbor J_2 and Dzyaloshinskii-Moriya exchanges. Both models feature zigzag antiferromagnetic order at zero magnetic field and a single phase transition under in-plane magnetic fields to a partially-polarized phase. Within the antiferromagnetic phase, Γ_B is found to be negative up to the critical fields (corresponding to the suppression of magnetic order B_c^{AF2}) near to 6 T. At these critical fields, a sign change in Γ_B occurs. The fact that Γ_B does not diverge at B_c^{AF2} and only shows a delayed maximum at higher field strengths is likely a finite-size effect of the calculation, as the gap cannot fully close at a continuous transition on a finite cluster. Various universal features found in our measurements are nevertheless captured qualitatively: The field strength at which the sign change takes place shows the correct dependence on the in-plane angle in both models (blue vertical lines in Fig. 6), with highest magnetic fields for $\phi = 0^\circ$ and lowest for $\phi = 30^\circ$. While model A shows no anomalies beyond the sign change and maximum in Γ_B, model B features shoulder anomalies at higher field strengths [orange vertical lines in Figs. 6(c) and 6(d)]. Such anomalies are found in various extended Kitaev models that are proximate to competing phases at finite fields but do not enter them [23]. They occur as a result of field-induced level crossings in the lowest excited states within the partially-polarized phase and appear as a negative jump in Γ_B for $T \to 0$ K that is smeared out at finite temperatures. In the present model B of Ref. [38], both the position of the sign change and that of the shoulder anomaly are found to shift to lower field strengths upon rotating from $\phi = 0^\circ$ to $\phi = 30^\circ$. This behavior is qualitatively consistent with the anomalies observed in experiment (Fig. 5), however, in the present set of *ab initio* parameters occurs at much higher field strengths. This might be a result of finite-size effects and/or could be refined by adjusting these parameters. We also checked the effect of magnetic fields perpendicular to the honeycomb plane ($\mathbf{B} \parallel c^*$) [black points in Fig. 6(a)]. In accordance with our measurement, the Grüneisen parameter is found to be approximately zero for this direction (up to field strengths of ∼33 T in model A).

IV. CONCLUSION

In summary, our comprehensive thermodynamic study of α-$RuCl_3$ revealed several universal features of this material that do not depend on the direction of the in-plane magnetic field. For the magnetically ordered phases $B \leqslant B_c^{\mathrm{AF2}}$, the phase boundary separating them from the quantum paramagnetic state is nonmonotonic, suggesting a narrow region of inverse melting. The in-plane anisotropy manifests itself in the different stability range of the intermediate ordered phase observed between B_c^{AF1} and B_c^{AF2}. For the quantum paramagnetic region $B > B_c^{\mathrm{AF2}}$, our data is clearly inconsistent with the existence of an additional continuous transition and also speaks against a first-order transition. This applies both for field angles where a gapless Kitaev spin liquid (KSL) and angles where a gapped KSL have been proposed, implying that the plateau in the thermal Hall conductivity in α-$RuCl_3$ does not go along with a topologically nontrivial KSL. Instead, the observed thermodynamics are qualitatively consistent with a single phase above B_c^{AF2} with a monotonically growing excitation gap.

ACKNOWLEDGMENTS

We thank Yoshi Tokiwa for his experimental assistance during early stages of this work. The research in Augsburg was supported by the German Research Foundation (DFG)

via the Project No. 107745057 (TRR80) and by the Federal Ministry for Education and Research through the Sofja Kovalevskaya Award of Alexander von Humboldt Foundation (AAT). The work in Frankfurt was supported by the DFG Project No. 411289067 (VA117/15-1). R.V. was supported in part by the National Science Foundation under Grant No. NSF PHY-1748958.

APPENDIX A: MORE DETAILS ABOUT Γ_B

Here, we present our Grüneisen parameter study in more detail. Figure 7 illustrates the whole field range from 0 to 14 T for the field applied along (a) [110] and (b) [010] at 1 and 2 K, respectively. As already discussed before, the main signatures result from B_c^{AF2} and B_c^{AF1}, the latter being weakest for [010]. The sign change due to an entropy maximum at ∼2 T from Ref. [23] is reproduced and likely related to domain reconstruction, as reported previously [11]. Now, we focus on establishing the temperature-field phase diagram from the main text (Fig. 2). In Fig. 8, all measured temperatures are shown for (a),(b) [110] and (c),(d) [010], respectively. Determining B_c^{AF2} as the transition from the AF to the field-polarized state is straightforward due to the obvious sign change from negative to positive. In contrast, B_c^{AF1} cannot always be identified with comparable accuracy. For [110] at temperatures up to 2.5 K, the maximum indicative of the first-order transition is clearly visible [arrows in Fig. 8(a)]. However, this maximum broadens towards higher temperatures and eventually becomes almost completely smeared out

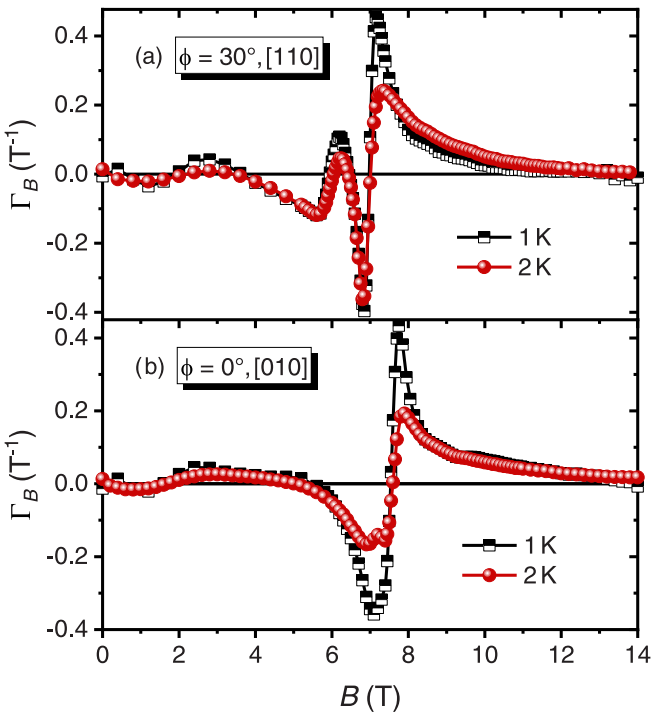

FIG. 7. Field dependence of the magnetic Grüneisen parameter Γ_B over the whole measured range from 0 to 14 T for the different field orientations (a) [110] and (b) [010], respectively. The main signatures are the transitions at B_c^{AF2} and B_c^{AF1}. The sign change at ∼2 T from Ref. [23] is reproduced and likely results from domain reconstruction [11].

at 4 K. At this point, B_c^{AF1} is defined by the remaining kink [arrow in Fig. 8(b)]. Above that temperature, even this kink fades away. With the field oriented along [010], establishing B_c^{AF1} is even more challenging because of the proximity to the dominant feature at B_c^{AF2}. At 1 K, B_c^{AF1} appears as a broad shoulder, which evolves into a maximum at higher temperatures, e.g., 2 K [arrows in Fig. 8(c)]. Yet, it cannot be identified any more below 1 K because, most likely, it becomes hidden by B_c^{AF2}. Nevertheless, our data cannot exclude the complete disappearance of B_c^{AF1} below 1 K. Similarly to $\vec{B} \parallel [110]$, the maximum transforms into a kink at higher temperatures [Fig. 8(d)] and eventually vanishes.

Finally, the field evolution of the Grüneisen parameter at 1 K and 500 mK is shown in Fig. 9 for several field orientations. At 1 K in Fig. 9(a), $\phi = 20^\circ$ reveals a plateau at a similar position like [010]. Furthermore, the weaker anisotropy along [010] is corroborated because rotating by $\phi = 5^\circ$ does not change $\Gamma_B(B)$ significantly compared to [010]. At 500 mK, the cell background cannot be subtracted as explained below. A minimal difference between $\phi = \pm 5^\circ$ directly below B_c^{AF2} might indicate that $\phi = 0^\circ$ is not perfectly aligned along [010]. Nonetheless, this misalignment should be smaller than 2°. Aside from this small deviation, the data for ± 5 and 0° are almost perfectly on top of each other, further confirming the weaker anisotropy along the [010] direction. Figure 9(c) represents the evolution above B_c^{AF2} in more detail. As described in the main text, the shoulder feature as a universal characteristic is visible for all field orientations. The measurements of $\phi = \pm 5^\circ$ confirm the probable appearance of a second shoulder anomaly for $\phi = 0^\circ$.

APPENDIX B: HEAT CAPACITY BELOW 1 K

In this part, we present field-dependent heat capacity measurements below 1 K. First, we focus on the phase transitions B_c^{AF1} and B_c^{AF2}. Second, we discuss the influence of nuclear contribution on the results above B_c^{AF2}. Finally, we conclude with a comment about the analysis at low temperatures and high fields in our setup and how this influences a potential determination of a small gap.

Figure 10(a) shows the field-dependent heat capacity of the α-$RuCl_3$ crystal at 500 mK for several directions in absolute units of μJ/K since no cell background subtraction was possible, as explained in more detail below. The phase transition at $B_c^{\mathrm{AF2}} \sim 7$–$7.6$ T is perfectly resolved as a peak for all field orientations. For [110], a second maximum indicative of B_c^{AF1} is clearly visible. In a similar manner, the heat capacity data at 200 mK and [110] orientation are interpreted [Fig. 10(b)]. Both B_c^{AF1} and B_c^{AF2} are undoubtedly identifiable.

Now, we return to the 500 mK data [Fig. 10(a)]. Towards higher fields a strange monotonic increase is observed; its origin will be discussed below. Notwithstanding this spurious effect, no additional anomaly can be seen above B_c^{AF2} for any field direction, also for the 200 mK data in the field along [110]. Therefore, we conclude that our heat capacity data show the absence of further transitions beyond B_c^{AF2} for all measured field directions.

In the following, we focus on the reason for the unphysical heat capacity behavior far above B_c^{AF2}. We attribute this to the presence of nuclear contribution in our setup. This

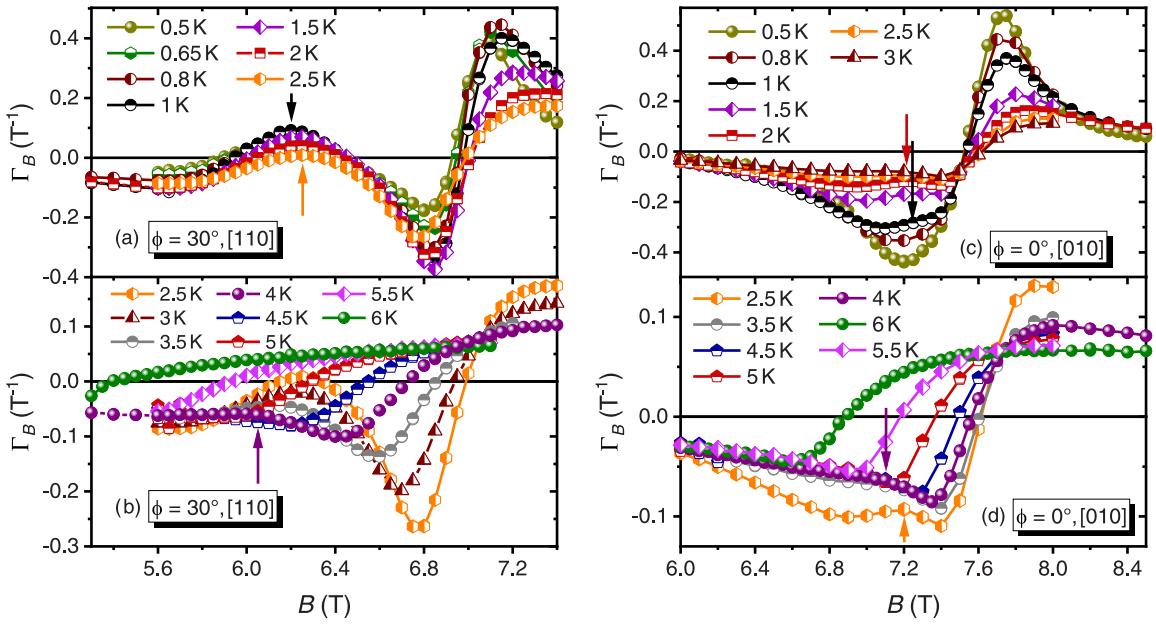

FIG. 8. Detailed Γ_B measurements used for the determination of B_c^{AF1} and B_c^{AF2} for (a), (b) $\vec{B} \parallel [110]$ and (c), (d) $\vec{B} \parallel [010]$. Raw data without cell background subtraction are shown, because corresponding specific heat data were not always available. This does not affect the positions of B_c^{AF1} and B_c^{AF2}, as explained in the text. The transition at B_c^{AF2} is easily identified as the sign change from negative to positive for all temperatures and field directions. (a), (b) [110] direction. The maximum indicative of B_c^{AF1} is clearly visible at temperatures below 2.5 K (black and orange arrow) and broadens toward higher temperatures transforming into a kink at 4 K (purple arrow), and finally vanishes. (c), (d) [010] direction. Here, the determination of B_c^{AF1} is hindered by the proximity to the dominant transition at B_c^{AF2}. The 2 K data show a maximum (red arrow) that develops into a broad shoulder at 1 K (black arrow), and becomes fully screened by the increasingly sharp feature at B_c^{AF2} toward lower temperatures. Above 2.5 K, the maximum becomes a kink (orange and purple arrow) and vanishes, similarly to the [110] orientation.

contribution is enhanced in high magnetic fields and becomes comparable to the small sample heat capacity in the order of several ∼10 nJ/K. Combined with a sizable spin-lattice relaxation time this may give rise to the so-called 2τ effect [45,46] and cause discrepancies when standard analysis with a single exponential function is used. Obviously, as shown in Figs. 10(c)–10(f), such deviations only occur at fields far beyond B_c^{AF2}, which is unambiguously visible in the logarithmic plots (insets). Consequently, the analysis using the single exponential function results in unreasonable behavior. We assign the nuclear contribution to the sapphire platform (Al_2O_3) due to the nuclear moments of Al because the background measurement without sample revealed very similar behavior. Accordingly, a precise analysis of the cell background was impossible, too, preventing a background subtraction in Figs. 10(a) and 10(b) as well as in 9(b) and 9(c).

As a result, due to this problem below 1 K and at high fields, our heat capacity data do not allow us

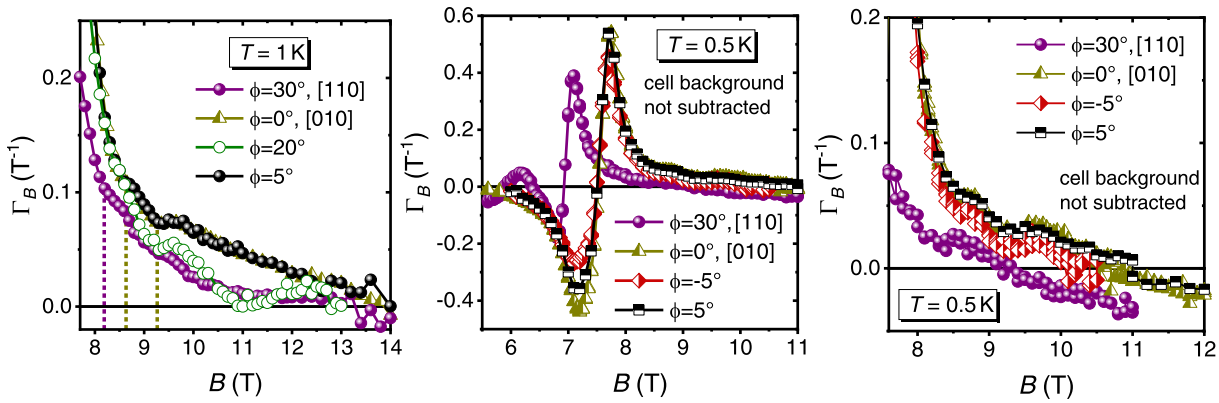

FIG. 9. Field dependence of Γ_B beyond B_c^{AF2} at the lowest measured temperatures. (a) More field directions at 1 K. (b) At 500 mK, no background subtraction is available due to the lack of $C(B)$. Nevertheless, both B_c^{AF1} and B_c^{AF2} are very well resolved for all field directions. As already shown previously, the subtraction of the background does not change the position of any anomaly in $\Gamma_B(B)$. (c) Zoom-in into Γ_B above B_c^{AF2}. Shoulderlike anomalies are visible being most pronounced for $\vec{B} \parallel [010]$.

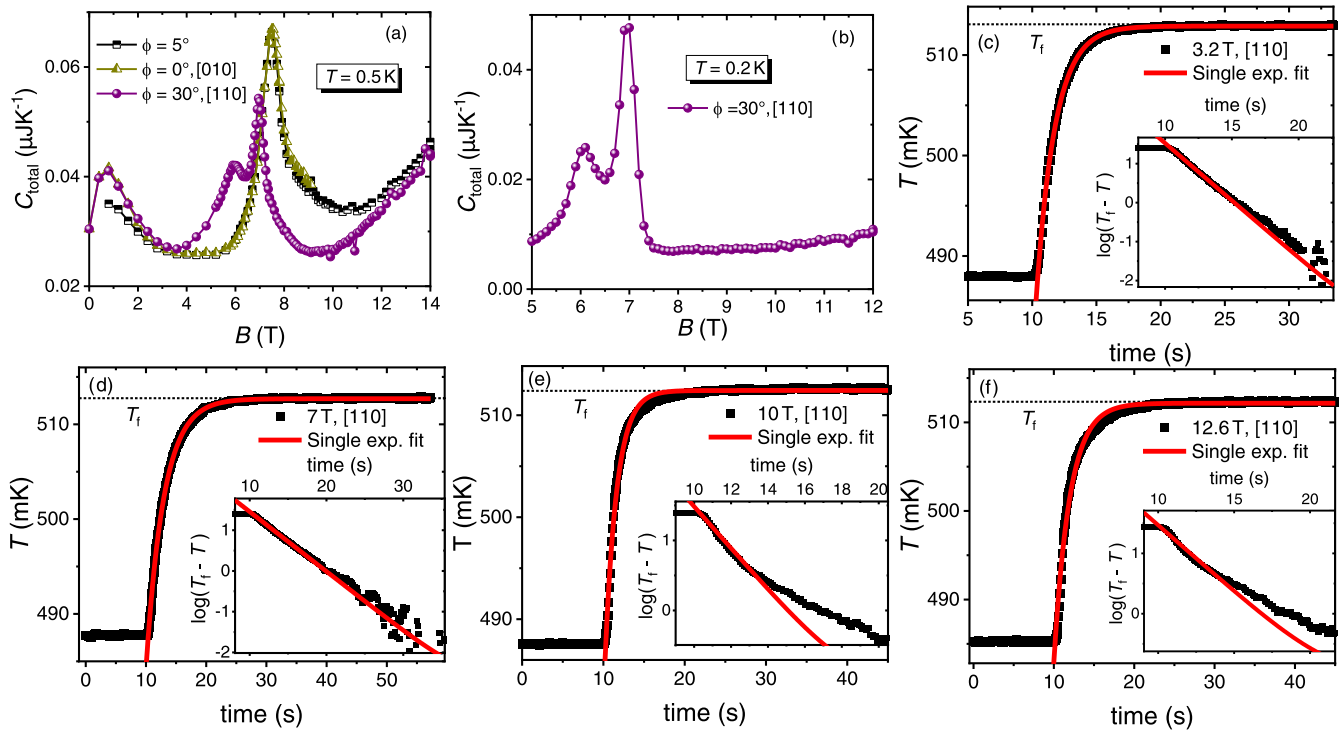

FIG. 10. (a) Field dependence of the total heat capacity C_{tot} (including background) up to 14 T for several field orientations. They perfectly match the 1 K data from the main text, undoubtedly resolving B_c^{AF2} and, in the case $\vec{B} \parallel [110]$, also B_c^{AF1}. Far above B_c^{AF2}, fitting with a single exponential function is not adequate anymore resulting in the unphysical increase towards higher fields due to shortcomings of the single exponential function analysis. Nevertheless, we speculate that a phase transition beyond B_c^{AF2} would give rise to a deviation from the monotonic behavior, e.g., in form of another peak. As a consequence, from these data, we suspect that a phase transition seems to be unlikely. (b) Heat capacity for $\vec{B} \parallel [110]$ at 200 mK. B_c^{AF1} and B_c^{AF2} are perfectly resolved while the monotonic behavior beyond B_c^{AF2} does not indicate any further phase transition. (c-f) Examples for the sample temperature response $T(t)$ at 500 mK and different magnetic fields, all applied along the [110] direction. A single exponential function describes $T(t)$ very well for lower fields of e.g. (a) 3.2 T and (b) 7 T, respectively. At higher fields well beyond the phase transition B_c^{AF2}, the single exponential fit obviously deviates from the data points at (c) 10 T and (d) 12.6 T, respectively. This is even more obvious in the logarithmic plot in the insets where two time constants are present, manifesting themselves in different slopes.

to determine the excitation gap under high magnetic fields. The framework beyond Refs. [45,46] would be needed to ensure an appropriate subtraction of the nuclear contribution.

[1] A. Kitaev, Anyons in an exactly solved model and beyond, Ann. Phys. **321**, 2 (2006).

[2] M. Hermanns, I. Kimchi, and J. Knolle, Physics of the Kitaev model: Fractionalization, dynamic correlations, and material connections, Annu. Rev. Condens. Matter Phys. **9**, 17 (2018).

[3] J. G. Rau, E. K.-H. Lee, and H.-Y. Kee, Spin-orbit physics giving rise to novel phases in correlated systems: Iridates and related materials, Annu. Rev. Condens. Matter Phys. **7**, 195 (2016).

[4] S. M. Winter, A. A. Tsirlin, M. Daghofer, J. van den Brink, Y. Singh, P. Gegenwart, and R. Valentí, Models and materials for generalized Kitaev magnetism, J. Phys.: Condens. Matter **29**, 493002 (2017).

[5] H. Takagi, T. Takayama, G. Jackeli, G. Khaliullin, and S. Nagler, Concept and realization of Kitaev quantum spin liquids, Nat. Rev. Phys. **1**, 264 (2019).

[6] A. Banerjee, C. A. Bridges, J.-Q. Yan, A. A. Aczel, L. Li, M. B. Stone, G. E. Granroth, M. D. Lumsden, Y. Yiu, J. Knolle, S. Bhattacharjee, D. L. Kovrizhin, R. Moessner, D. A. Tennant, D. G. Mandrus, and S. E. Nagler, Proximate Kitaev quantum spin liquid behavior in a honeycomb magnet, Nat. Mater. **15**, 733 (2016).

[7] A. Banerjee, J. Yan, J. Knolle, C. A. Bridges, M. B. Stone, M. D. Lumsden, D. G. Mandrus, D. A. Tennant, R. Moessner, and S. E. Nagler, Neutron scattering in the proximate quantum spin liquid α-$RuCl_3$, Science **356**, 1055 (2017).

[8] G. Bastien, G. Garbarino, R. Yadav, F. J. Martinez-Casado, R. Beltrán Rodríguez, Q. Stahl, M. Kusch, S. P. Limandri, R. Ray, P. Lampen-Kelley, D. G. Mandrus, S. E. Nagler, M. Roslova, A. Isaeva, T. Doert, L. Hozoi, A. U. B. Wolter, B. Büchner, J. Geck, and J. van den Brink, Pressure-induced dimerization and valence bond crystal formation in the Kitaev-Heisenberg magnet α-$RuCl_3$, Phys. Rev. B **97**, 241108(R) (2018).

[9] T. Biesner, S. Biswas, W. Li, Y. Saito, A. Pustogow, M. Altmeyer, A. U. B. Wolter, B. Büchner, M. Roslova,

T. Doert, S. M. Winter, R. Valentí, and M. Dressel, Detuning the honeycomb of α-$RuCl_3$: Pressure-dependent optical studies reveal broken symmetry, Phys. Rev. B **97**, 220401(R) (2018).

[10] P. Lampen-Kelley, A. Banerjee, A. A. Aczel, H. B. Cao, M. B. Stone, C. A. Bridges, J.-Q. Yan, S. E. Nagler, and D. Mandrus, Destabilization of Magnetic Order in a Dilute Kitaev Spin Liquid Candidate, Phys. Rev. Lett. **119**, 237203 (2017).

[11] J. A. Sears, Y. Zhao, Z. Xu, J. W. Lynn, and Y.-J. Kim, Phase diagram of α-$RuCl_3$ in an in-plane magnetic field, Phys. Rev. B **95**, 180411(R) (2017).

[12] S.-H. Baek, S.-H. Do, K.-Y. Choi, Y. S. Kwon, A. U. B. Wolter, S. Nishimoto, J. van den Brink, and B. Büchner, Evidence for a Field-Induced Quantum Spin Liquid in α-$RuCl_3$, Phys. Rev. Lett. **119**, 037201 (2017).

[13] A. Banerjee, P. Lampen-Kelley, J. Knolle, C. Balz, A. A. Aczel, B. Winn, Y. Liu, D. Pajerowski, J. Yan, C. A. Bridges, A. T. Savici, B. C. Chakoumakos, M. D. Lumsden, D. A. Tennant, R. Moessner, D. G. Mandrus, and S. E. Nagler, Excitations in the field-induced quantum spin liquid state of α-$RuCl_3$, npj Quantum Mater. **3**, 8 (2018).

[14] Y. Kasahara, T. Ohnishi, Y. Mizukami, O. Tanaka, S. Ma, K. Sugii, N. Kurita, H. Tanaka, J. Nasu, Y. Motome, T. Shibauchi, and Y. Matsuda, Majorana quantization and half-integer thermal quantum Hall effect in a Kitaev spin liquid, Nature (London) **559**, 227 (2018).

[15] A. Sahasrabudhe, D. A. S. Kaib, S. Reschke, R. German, T. C. Koethe, J. Buhot, D. Kamenskyi, C. Hickey, P. Becker, V. Tsurkan, A. Loidl, S. H. Do, K. Y. Choi, M. Grüninger, S. M. Winter, Z. Wang, R. Valentí, and P. H. M. van Loosdrecht, High-field quantum disordered state in α-$RuCl_3$: Spin flips, bound states, and multiparticle continuum, Phys. Rev. B **101**, 140410(R) (2020).

[16] A. N. Ponomaryov, L. Zviagina, J. Wosnitza, P. Lampen-Kelley, A. Banerjee, J.-Q. Yan, C. A. Bridges, D. G. Mandrus, S. E. Nagler, and S. A. Zvyagin, Nature of Magnetic Excitations in the High-Field Phase of α-$RuCl_3$, Phys. Rev. Lett. **125**, 037202 (2020).

[17] P. A. Maksimov and A. L. Chernyshev, Rethinking α-$RuCl_3$, Phys. Rev. Research **2**, 033011 (2020).

[18] Throughout the paper, we discuss the Kitaev model and α-$RuCl_3$ in the framework of C_6 symmetry within the honeycomb lattice, implying that field angles are equivalent up to rotations of 60°. This symmetry is likely only approximately present for α-$RuCl_3$ in its $C2/m$ structure.

[19] T. Yokoi, S. Ma, Y. Kasahara, S. Kasahara, T. Shibauchi, N. Kurita, H. Tanaka, J. Nasu, Y. Motome, C. Hickey, S. Trebst, and Y. Matsuda, Half-integer quantized anomalous thermal Hall effect in the Kitaev material α-$RuCl_3$, arXiv:2001.01899.

[20] L. E. Chern, E. Z. Zhang, and Y. B. Kim, Sign structure of thermal Hall conductivity for in-plane-field polarized Kitaev magnets, arXiv:2008.12788.

[21] O. Tanaka, Y. Mizukami, R. Harasawa, K. Hashimoto, N. Kurita, H. Tanaka, S. Fujimoto, Y. Matsuda, E.-G. Moon, and T. Shibauchi, Thermodynamic evidence for field-angle dependent Majorana gap in a Kitaev spin liquid, arXiv:2007.06757.

[22] R. Schönemann, S. Imajo, F. Weickert, J. Yan, D. G. Mandrus, Y. Takano, E. L. Brosha, P. F. S. Rosa, S. E. Nagler, K. Kindo, and M. Jaime, Thermal and magnetoelastic properties of α-$RuCl_3$ in the field-induced low-temperature states, Phys. Rev. B **102**, 214432 (2020).

[23] S. Bachus, D. A. S. Kaib, Y. Tokiwa, A. Jesche, V. Tsurkan, A. Loidl, S. M. Winter, A. A. Tsirlin, R. Valentí, and P. Gegenwart, Thermodynamic Perspective on Field-Induced Behavior of α-$RuCl_3$, Phys. Rev. Lett. **125**, 097203 (2020).

[24] Y. Tokiwa and P. Gegenwart, High-resolution alternating-field technique to determine the magnetocaloric effect of metals down to very low temperatures, Rev. Sci. Inst. **82**, 013905 (2011).

[25] C. Balz, L. Janssen, P. Lampen-Kelley, A. Banerjee, Y. Liu, J. Yan, D. Mandrus, M. Vojta, and S. E. Nagler, Field-induced intermediate ordered phase and anisotropic interlayer interactions in α-$RuCl_3$, arXiv:2012.15258.

[26] S. Reschke, F. Mayr, S. Widmann, H.-A. Krug von Nidda, V. Tsurkan, M. V. Eremin, S.-H. Do, K.-Y. Choi, Z. Wang, and A. Loidl, Sub-gap optical response in the Kitaev spin-liquid candidate α-$RuCl_3$, J. Phys.: Condens. Matter **30**, 475604 (2018).

[27] R. D. Johnson, S. C. Williams, A. A. Haghighirad, J. Singleton, V. Zapf, P. Manuel, I. I. Mazin, Y. Li, H. O. Jeschke, R. Valentí, and R. Coldea, Monoclinic crystal structure of α-$RuCl_3$ and the zigzag antiferromagnetic ground state, Phys. Rev. B **92**, 235119 (2015).

[28] M. Majumder, M. Schmidt, H. Rosner, A. A. Tsirlin, H. Yasuoka, and M. Baenitz, Anisotropic $Ru^{3+}4d^5$ magnetism in the α-$RuCl_3$ honeycomb system: Susceptibility, specific heat, and zero-field NMR, Phys. Rev. B **91**, 180401(R) (2015).

[29] K. Riedl, Y. Li, S. M. Winter, and R. Valentí, Sawtooth Torque in Anisotropic $j_{\text{eff}} = \frac{1}{2}$ Magnets: Application to α-$RuCl_3$, Phys. Rev. Lett. **122**, 197202 (2019).

[30] K. Hui, Reentrant behavior of an in-plane antiferromagnet in a magnetic field, Phys. Rev. B **38**, 802 (1988).

[31] N. Schupper and N. M. Shnerb, Inverse melting and inverse freezing: A spin model, Phys. Rev. E **72**, 046107 (2005).

[32] W. E. F. Parente, J. T. M. Pacobahyba, I. G. Araújo, M. A. Neto, J. Ricardo de Sousa, and U. Akinci, Critical and reentrant behavior of the spin quantum 1/2 anisotropic Heisenberg antiferromagnet model with Dzyaloshinskii-Moriya interaction in a longitudinal magnetic field, J. Magn. Magn. Mater. **355**, 235 (2014).

[33] K. Ran, J. Wang, W. Wang, Z.-Y. Dong, X. Ren, S. Bao, S. Li, Z. Ma, Y. Gan, Y. Zhang, J. T. Park, G. Deng, S. Danilkin, S. -L. Yu, J.-X. Li, and J. Wen, Spin-Wave Excitations Evidencing the Kitaev Interaction in Single Crystalline α-$RuCl_3$, Phys. Rev. Lett. **118**, 107203 (2017).

[34] To estimate an *upper* bound of magnetic entropy for an antiferromagnetic phase with gap Δ, one may consider completely flat magnon bands with energy $E(\mathbf{q}) = \Delta$. For $\Delta = 1.5$ meV and $T = 1$ K this leads to $S_{\text{max}} \approx 0.0042$ mJ mol^{-1} K^{-1}.

[35] C. Wellm, J. Zeisner, A. Alfonsov, A. U. B. Wolter, M. Roslova, A. Isaeva, T. Doert, M. Vojta, B. Büchner, and V. Kataev, Signatures of low-energy fractionalized excitations in α-$RuCl_3$ from field-dependent microwave absorption, Phys. Rev. B **98**, 184408 (2018).

[36] R. Hentrich, X. Hong, M. Gillig, F. Caglieris, M. Čulo, M. Shahrokhvand, U. Zeitler, M. Roslova, A. Isaeva, T. Doert, L. Janssen, M. Vojta, B. Büchner, and C. Hess, High-field thermal transport properties of the Kitaev quantum magnet α-$RuCl_3$: Evidence for low-energy excitations beyond the critical field, Phys. Rev. B **102**, 235155 (2020).

[37] S. Gass, P. M. Cônsoli, V. Kocsis, L. T. Corredor, P. Lampen-Kelley, D. G. Mandrus, S. E. Nagler, L. Janssen, M. Vojta, B. Büchner, and A. U. B. Wolter, Field-induced transitions in the Kitaev material α-$RuCl_3$ probed by thermal expansion and magnetostriction, Phys. Rev. B **101**, 245158 (2020).

[38] D. A. S. Kaib, S. Biswas, K. Riedl, S. M. Winter, and R. Valentí, Magnetoelastic coupling and effects of uniaxial strain in α-$RuCl_3$ from first principles, arXiv:2008.08616.

[39] M. Yamashita, J. Gouchi, Y. Uwatoko, N. Kurita, and H. Tanaka, Sample dependence of half-integer quantized thermal Hall effect in the Kitaev spin-liquid candidate α-$RuCl_3$, Phys. Rev. B **102**, 220404(R) (2020).

[40] C. Balz, P. Lampen-Kelley, A. Banerjee, J. Yan, Z. Lu, X. Hu, S. M. Yadav, Y. Takano, Y. Liu, D. A. Tennant, M. D. Lumsden, D. Mandrus, and S. E. Nagler, Finite field regime for a quantum spin liquid in α-$RuCl_3$, Phys. Rev. B **100**, 060405(R) (2019).

[41] M. Garst and A. Rosch, Sign change of the Grüneisen parameter and magnetocaloric effect near quantum critical points, Phys. Rev. B **72**, 205129 (2005).

[42] D. Wulferding, Y. Choi, S.-H. Do, C. Lee, P. Lemmens, C. Faugeras, Y. Gallais, and K.-Y. Choi, Magnon bound states versus anyonic Majorana excitations in the Kitaev honeycomb magnet α-$RuCl_3$, Nat. Commun. **11**, 1603 (2020).

[43] S. M. Winter, K. Riedl, D. Kaib, R. Coldea, and R. Valentí, Probing α-$RuCl_3$ Beyond Magnetic Order: Effects of Temperature and Magnetic Field, Phys. Rev. Lett. **120**, 077203 (2018).

[44] S. M. Winter, K. Riedl, P. A. Maksimov, A. L. Chernyshev, A. Honecker, and R. Valentí, Breakdown of magnons in a strongly spin-orbital coupled magnet, Nat. Commun. **8**, 1152 (2017).

[45] B. Andraka and Y. Takano, Simultaneous measurements of heat capacity and spin-lattice relaxation time in high magnetic field at low temperature, Rev. Sci. Instrum. **67**, 4256 (1996).

[46] B. Andraka and Y. Takano, Note: Relaxation heat capacity measurements at low temperatures: Dealing with nuclear contribution, Rev. Sci. Instrum. **82**, 016103 (2011).